




Understanding the role of neutral species by means of high-order interaction in the rock-paper-scissors dynamics

Yikang Lu ^{1,2} Xiaoyue Wang,¹ Chunpeng Du,³ Yanan Wang,^{2,4} Yini Geng,⁵ Lei Shi ^{1,6,*} and Junpyo Park ^{7,†}

¹*School of Statistics and Mathematics, Yunnan University of Finance and Economics, Kunming, Yunnan 650221, China*

²*Institute for Biocomputation and Physics of Complex Systems, University of Zaragoza, 50018 Zaragoza, Spain*

³*School of Mathematics, Kunming University, Kunming, 650214, China*

⁴*School of Economics and Management, Beihang University, Beijing 100191, China*

⁵*School of Mathematics and Statistics, Hunan Normal University, Changsha 410081, China*

⁶*Interdisciplinary Research Institute of Data Science, Shanghai Lixin University of Accounting and Finance, Shanghai 201209, China*

⁷*Department of Applied Mathematics, College of Applied Sciences, Kyung Hee University, Yongin 17104, Republic of Korea*



(Received 2 March 2023; accepted 5 January 2024; published 29 January 2024)

The existence of neutral species carries profound ecological implications that warrant further investigation. In this paper, we study the impact of neutral species on biodiversity in a spatial tritrophic system of cyclic competition, in which the neutral species are identified as the fourth species that may affect the competition process of the other three species under the rock-paper-scissors (RPS) rule. Extensive simulations showed that neutral species can promote coexistence in a high mobility regime within the system. When coexistence occurs, we found that the state can be maintained by two mechanisms: Species can either (i) adhere to traditional RPS rule or (ii) form patches to resist invasion. Our findings might aid in understanding the impact of neutral species on biodiversity in ecosystems.

DOI: [10.1103/PhysRevE.109.014313](https://doi.org/10.1103/PhysRevE.109.014313)

I. INTRODUCTION

Higher-order interaction (HOI) is pervasive in society and ecology [1–4]. It is well established that HOIs play an essential role in the species coexistence within natural plant communities [1] and closed and open ecological communities [5]. In addition, to a vast extent, HOI can reflect the synergistic effects of multiple species. For these reasons, HOIs and their dynamics have attracted much attention over the past decade [5–8].

In existing models for HOI studies, a recent study [8] introduced three interaction models: (a) pairwise interaction, (b) three-way interaction, and (c) four-way interaction. In the context of pairwise interaction, the third species does not exert any influence on the dynamics of the other two species, a scenario akin to a rock-paper-scissors (RPS) game in which each of the three species dominates one species and is dominated by the other [9–13]. When a third species influences the interaction dynamics between two other species, whether the third species exerts a favorable or adverse impact, this phenomenon is referred to as a three-way interaction. In the case of four-way interactions, the presence of the fourth species modulates how the third species interferes with pairwise interactions.

RPS is a widely recognized example of a nonhierarchical competitive game observed in various contexts, e.g., side-blotched lizard populations [14], coral reef invertebrates [15], and mutant yeast strains [16]. This competitive relationship

demonstrates that three or more species cyclically interact with each other without any clear hierarchy or dominance among them [17]. The classic RPS game is portrayed as a critical paradigm for nonhierarchically cyclic competition in structured populations. It has been studied in various frameworks to capture the influence of species coexistence based on pairwise interaction, such as intraspecific and interspecific competition [18–22], interactive models [23–25], and species mortality [26]. It is also found that breaking the one-way invasive direction does not promote coexistence [27], and the weakest species promotes coexistence and dominates, as predicted by simulations and theory and confirmed in actual experiments [22,28,29]. Furthermore, researchers have investigated the perturbation of the structurally intransitive cycle of N species. Chatterjee *et al.* conducted a study with the aim of understanding the influence of biodiversity in the presence of HOIs [30]. Their research explored the impact of perturbations on species coexistence and dominance, shedding light on the dynamics of ecosystems characterized by nonhierarchical competition.

The three-way interaction in Fig. 1 is a generally existing phenomenon in nature. *Arbuscular mycorrhizal* fungi not only promote the growth of *Plantago lanceolata* but also enhance the development of its competitor, *Panicum sphaerocarpon* [31]. In addition, elephants acquire sustenance by browsing shrubs and trees, which can yield indirect advantages for other fauna. The act of elephant browsing induces modifications in the vegetation structure, leading to dense thickets or shrubby patches. These vegetative alterations offer concealment and refuge for diminutive organisms, including small mammals, birds, and reptiles [32]. On the other hand, there are two

*shi_lei65@hotmail.com

†junpyopark@khu.ac.kr

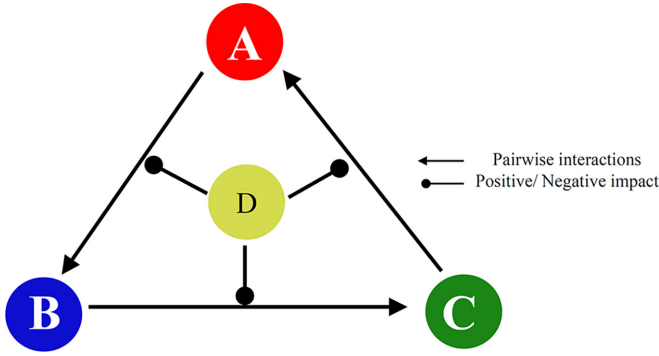


FIG. 1. Schematic diagram of rock-paper-scissors dynamics with neutral species. Species A , B , and C participate in the game, and D is the neutral species.

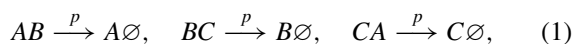
typical examples when we consider four species: (a) four species form competition in cycles and (b) an additional species engaging in the competition process, such as pestilent species and apex predators are involved. Even if altering the invasion strength of pestilent species, the coexistence is not necessarily broken [33]. Introducing apex predators in the RPS system, competition always occurs at a rate below reproduction, while high-density apex predators cause the entire system to collapse [34].

In this paper, we introduce a fourth species, which serves as a neutral element within our system and can modulate species competition. To be specific, a parameter γ , governing the modulation of competition rates due to the density fluctuations of neutral species, can exert an impact on interspecific competition among the three species under the RPS mechanism. This suggests that species can play both negative and positive roles, the nature of which can be defined by the sign of γ . In addition, through extensive simulations, we found that coexistence is still maintained at the high mobility regime, even if the additional species are considered. We demonstrate that the presence of neutral species with high density promotes coexistence, as basin entropy increases with increasing γ .

In Sec. II, we describe the spatial RPS game with the neutral species. In Sec. III, we present results on biodiversity under the presence of neutral species with various densities showing spatiotemporal simulations and the extinction probability and provide basin entropy to support such numerical findings. The paper is concluded in Sec. IV with a discussion in a broader aspect.

II. MODEL

On spatially extended systems, the RPS game is generally explored on a square lattice of size $N = L \times L$ with periodic boundaries in which three species A , B , C , and empty sites \emptyset are randomly distributed. Then species, including empty sites, can interact with the nearest-neighboring sites by following the reaction rules:



where X and Y are one of the species or an empty site.

To realize the HOI among three cyclically competing species based on the model in Fig. 1, we consider the fourth species (referred to as D) as a neutral species to affect interspecific competition among three species. Since species D is a neutral species, it will not participate in the cyclic competition but can do the exchange process (3). Here, we initially assign ρ ($\rho > 0$) as the density of D .

Reaction (1) describes interspecific competition among three species with a rate p as usual, but there is a difference compared to prior studies [12,18,19]. Since the species interactions, neither predators nor prey, are affected by neutral species D rather than using a constant, the rate p for the interspecific competition is defined in a different way: $p = \exp(\gamma \rho_i / k)$, in which γ reflects the sensitivity to the number of D in the nearest neighborhood of node i , ρ_i . This equation is designed to maintain a competition rate that is consistently greater than zero and reflects the phenomenon where an increase in the density of neutral species results in a pronounced shift in the competition rate. To be concrete, for $\gamma = 0$, the model falls into the classic system of RPS [35]. On the other hand, the nonzero γ can propose valuable meanings: A smaller γ or a larger ρ_i indicates a stronger inhibitory effect of D for $\gamma < 0$ and D plays a positive role in the competition for $\gamma > 0$. The k is the degree of node i and is given as 4 since our square lattice is considered to have a von Neumann neighboring structure. Reactions (2) and (3) demonstrate reproduction and exchange with rates q and ε , respectively, as usual, in which the rate ε is defined by $\varepsilon = 2MN$ with a size of square lattice N and mobility M according to the theory of random walks [36]. To make an unbiased comparison with previous works [9,35], we assume the reproduction rate as the unity: $q = 1$.

In our simulations, we employ the Monte Carlo method as follows. On a square lattice of sizes ranging from $N = 100 \times 100$ to 300×300 , we first introduce species D with a density ρ that is randomly distributed. At the same time, with the density of $1 - \rho$, the remaining sites are randomly occupied by one of species A , B , C , and empty sites \emptyset . Second, we arbitrarily select a pair of neighboring sites to interact with each other where one is active and the other is inactive. Third, reactions (1)–(3) will occur with normalized probabilities: $p/(p + q + \varepsilon)$, $q/(p + q + \varepsilon)$, and $\varepsilon/(p + q + \varepsilon)$, respectively. Note that the reproductive process will not occur when neighboring sites have no empty sites. When the selected pair contains D , the exchange process is only allowed with the probability $\varepsilon/(p + q + \varepsilon)$. One generation is defined by repeating the above process N times. Finally, we repeat the second and third steps above during T generations and set the total simulation time as $T = 8N$.

III. RESULTS

The presence of neutral species may play a positive role on the survival of other species. To investigate how neutral species can affect species biodiversity, we carried out numerical simulations within two distinct frameworks: Pattern formations and the extinction probability, which are the classic and traditional points to focus on in cyclic competition studies.

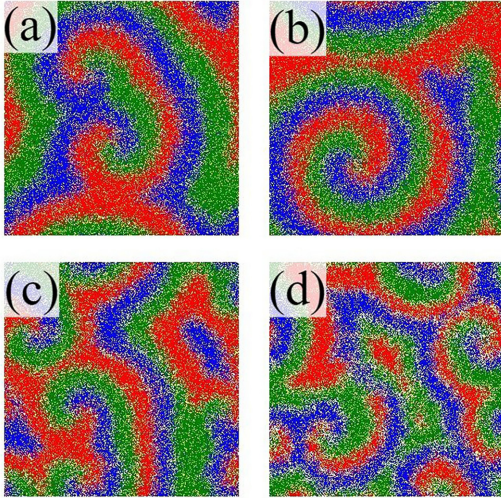


FIG. 2. Typical snapshots for fixed parameters $M = 10^{-4}$ and $\rho = 0.1$ with different γ : (a) -5 , (b) -2 , (c) 2 , and (d) 5 , which are obtained from the 712 200th time step. Four species A, B, C, D , and empty sites are represented by different colors: Red, blue, green, yellow, and white, respectively. As γ increases, the spiral patterns seem different.

A. Characteristics of pattern formations and biodiversity

On square lattices of size $N = 300 \times 300$, we first explored the evolution of biodiversity, in particular, considering the emergence of coexistence where possible for various γ under two different ρ : $\rho = 0.1$ and 0.7 , with the fixed mobility values $M = 10^{-5}$ and $M = 10^{-4}$. For the sake of brevity, the results pertaining to $M = 10^{-5}$ are presented in Appendix B.

Figure 2 presents illustrative snapshots from a lattice simulation involving $M = 10^{-4}$ and $\rho = 0.1$, each corresponding to different values of γ . Due to the inherent stochastic nature of random walks, the presence of species designated as D (depicted as yellow nodes) is subtle in each panel. However, the significance of the role played by D remains undeniable. More specifically, an increase in γ increases the intensity of interspecific competition among three species and thus generates more empty sites. In addition, as shown in Fig. 2, the value of γ affects the spatial pattern formation. When D plays a negative role, the observed pattern exhibits a higher degree of regularity. An interesting feature in pattern formations can be observed when γ is negative. To be concrete, as shown in Fig. 2(a), the spatial pattern exhibits a double spiral-wave state. In comparison, weakening the negative effect of D further, focusing on $\gamma = -2$ [see Fig. 2(b)], and the spatial pattern presents a single-armed spiral. On the other hand, for $\gamma > 0$, spirals become discontinuous, as shown in Figs. 2(c) and 2(d).

To further facilitate the comprehensive analysis of the process dynamics, we present evolution in the fraction of species as shown in Fig. 3 that corresponds to Fig. 2. The evolution of the density of species A, B, C , and empty sites, namely, ρ_A, ρ_B, ρ_C , and ρ_E , respectively, satisfies the mass conservation property of the system $\rho_A + \rho_B + \rho_C + \rho_E = 0.9$. Following prior findings [17,23], the density of the three species demonstrates persistent periodic oscillations even under the influence of minor interferences from neutral species. This observation serves

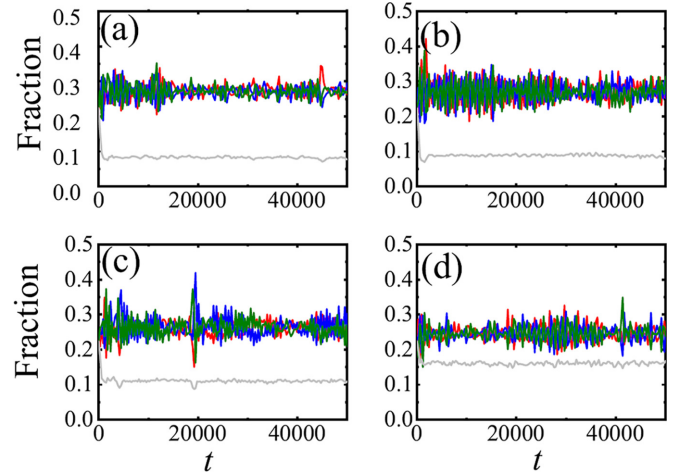


FIG. 3. Time-dependent evolution of densities with $M = 10^{-4}$ and $\rho = 0.1$ for different γ : (a) -5 , (b) -2 , (c) 2 , and (d) 5 . Red, blue, green, and grey lines represent species A, B, C , and empty sites. The increase in γ intensifies interspecific competition and consequently increases the fraction of empty sites.

as a manifestation of cyclic competitive dynamics. As the parameter γ increases, it engenders intensified competition among species, resulting in an augmented number of vacant sites and a reduction in species density other than the neutral species. The observed increase in white sites in Figs. 2(a)–2(d) further corroborates the conclusion above.

Furthermore, our attention is directed towards the occurrence of double spiral waves, as evident in Fig. 2(a). However, it's important to note that double spiral-wave formations are a rare sight in the context of the random distribution of individuals. Under the settings in our model, it is common for more than one double spiral to form. Therefore, we need to investigate the formation mechanism by observing evolutionary snapshots as shown in Fig. 4.

In Fig. 4(a), we can observe the random distribution of individuals at the beginning of the simulation. As the

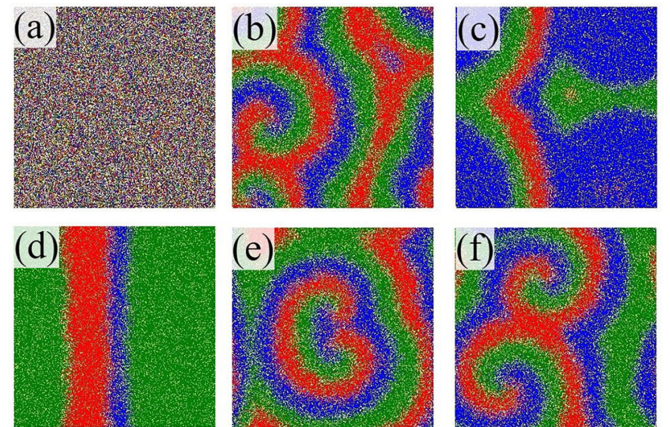


FIG. 4. Evolutionary snapshots for fixed parameters $M = 10^{-4}$, $\gamma = -2$, and $\rho = 0.1$ with different time steps: (a) 1, (b) 1 200 000, (c) 1 393 000, (d) 1 430 000, (e) 1 699 000, and (f) 1 900 000. Forming a strip wave only creates a group of double spiral waves.

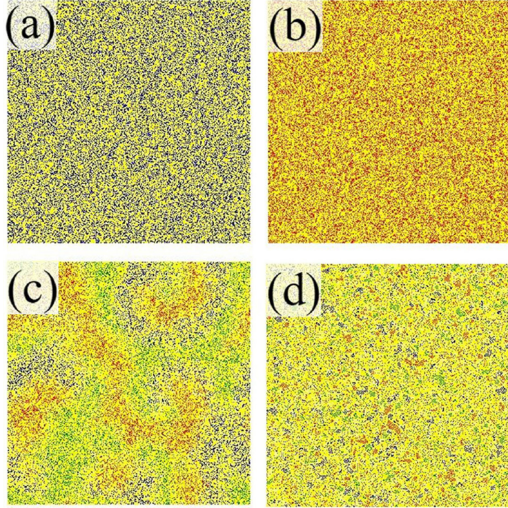


FIG. 5. Typical snapshots for fixed parameters $M = 10^{-4}$ and $\rho = 0.7$. The time step and a panel construction of γ are the same as Fig. 2. Since the density of D is moderately high, all panels seem occupied by it. In this case, the spatial patterns transfer from order to disorder as γ increases.

simulation progresses, the system evolves to develop a spiral pattern, as depicted in Fig. 4(b). Subsequently, species start to aggregate, giving rise to strip-wave patterns [as demonstrated in Figs. 4(c) and 4(d)]. These strip-wave patterns serve as the foundation for the formation of the double spiral waves.

It's worth noting that even when mobility remains constant, altering the density of species D can result in distinct pattern formations, as exemplified in Fig. 5 with $\rho = 0.7$. In this scenario, species engaged in cyclic competition find themselves surrounded by D . For low values of γ , these species face the risk of extinction, as illustrated in Figs. 5(a) and 5(b). In contrast, the pattern formations in the system are considerably different for $\gamma > 0$, as shown in Figs. 5(c) and 5(d). Specifically, for $\gamma = 2$, the species patches are randomly distributed across the network. As γ increases further up to 5, the species patches decrease, and all species are randomly distributed throughout the domain [see Fig. 5(d)]. The cluster formed by $\gamma = 2$ is greater than that formed by $\gamma = 5$.

Figure 5 reveals a notable pattern consisting of four species and empty sites. To further analyze the species' behavior, we analyze the evolution of the density of species. Due to the mass conservation property of the system, characterized by $\rho_A + \rho_B + \rho_C + \rho_E = 0.3$, as shown in Fig. 6, the scales observed in the fraction of species remain relatively small. In Figs. 6(a) and 6(b), following a substantial period of fluctuations, it becomes evident that species C and A marked by green and red gain dominance, resulting in the extinction of species other than the neutral species. Under this condition, the dominance of a particular species causes the fraction of empty sites to approach zero. Figures 5(c) and 6(c) indicate that coexistence becomes possible by the presence of large-scale, intricately interacting, and competing clusters through a circular competition method. For $\gamma = 5$, with the intensification of competitive intensity, the population clustering is significantly weakened and effectively segregated by the presence of neutral species, as depicted in Fig. 5(d). As a

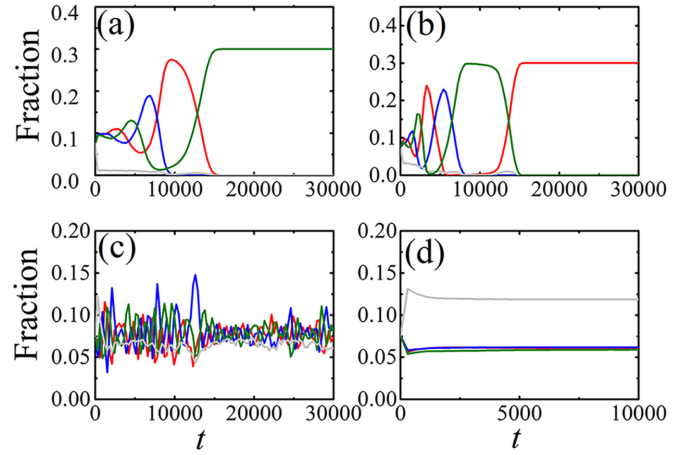


FIG. 6. Time-dependent evolution of densities with $M = 10^{-4}$ and $\rho = 0.7$ for different γ : (a) -5 , (b) -2 , (c) 2 , and (d) 5 . Red, blue, green, and grey lines represent species A , B , C , and empty sites. The increase in γ intensifies interspecific competition and consequently increases the fraction of empty sites.

consequence, this segregation results in a significant reduction in species density fluctuations, as illustrated in Fig. 6(d). As the competitive intensity intensifies, it is worth noting that the effect is relatively weaker in the case of $\gamma = 2$ compared to $\gamma = 5$. Consequently, the fraction of empty sites generated at $\gamma = 2$ is relatively lower than that observed in the case of $\gamma = 5$.

Meanwhile, there is one point we should note as we observe Fig. 5. As shown in Fig. 5, most situations have no spiral patterns. It is ambiguous whether spirals can emerge during the procedure compared to other snapshots taken under the same conditions. To uncover this ambiguity, we further explore the evolutionary snapshots for pattern formations depending on different time steps, as presented in Fig. 7.

We present typical snapshots obtained at specific parameter values: $M = 10^{-4}$, $\gamma = -2$, and $\rho = 0.7$. It is worth noting that this configuration drives species extinctions. We present

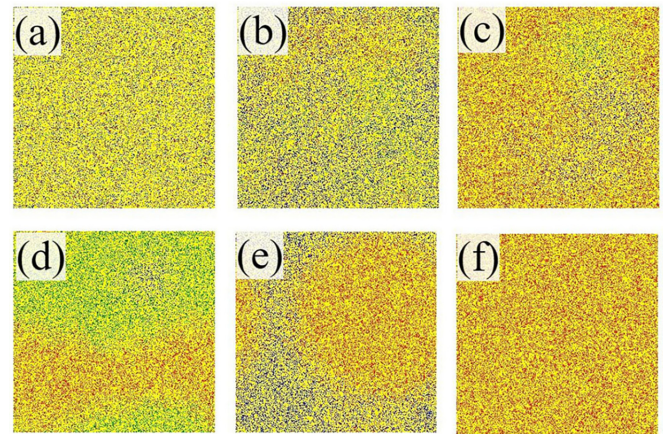


FIG. 7. Typical snapshots for fixed parameters $M = 10^{-4}$, $\gamma = -2$, and $\rho = 0.7$ at different time steps: (a) 1, (b) 23 000, (c) 193 000, (d) 2 260 000, (e) 2 330 000, and (f) 2 400 000. Species participating in the RPS game are embedded in D to form patches.

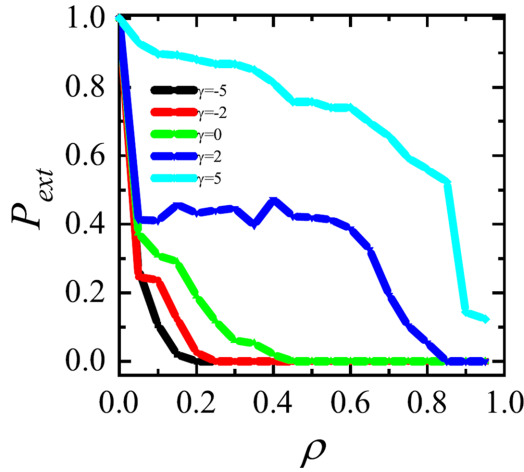


FIG. 8. Extinction probability P_{ext} as a function of ρ with different γ for $M = 0.1$. In each panel, different colors, black, red, green, blue, and cyan indicate different γ : -5 , -2 , 0 , 2 , and 5 , respectively. Neutral species contribute to the coexistence of species.

snapshots showcasing competition dynamics. Figure 7(a) illustrates the initial distribution of five different statuses. Due to the high density of yellow nodes, they consistently dominate the system. Other species and empty sites available primarily occupy the remaining space. Figures 7(b)–7(d) depict the sequential dominance of species B , A , and C (blue, red, and green nodes) within the available space. Figure 7(e) illustrates the gradual destruction of species C (green node) by species B (blue node). Finally, in Fig. 7(f), species A (red node), acting as the predator of species B (blue node), occupies the remaining space.

From Fig. 2 to Fig. 7, our investigation delved into biodiversity through the analysis of snapshots and the evolutionary dynamics of various species. To undertake a more comprehensive examination of the impact of neutral species density on biodiversity, we illustrate the probability of extinction (P_{ext}) as a function of ρ for $M = 0.1$. As depicted in Fig. 8, a higher neutral species density correlates with an enhanced level of biodiversity.

According to the aforementioned snapshots, species coexistence can always be maintained at the proper parameters regardless of the value of ρ . The coexistence mechanism is consistent with the traditional RPS model at low densities of D [9,11,22,25]. In addition, for the dense state of D , individuals belonging to the same species come together to form a patch. This mechanism is similar to that in an evolution game, where a patch of cooperators clings to resist the invasion of defectors [37,38].

The transition from Fig. 2 to Fig. 7 underscores the pronounced influence of the parameter γ on the proportion of vacant sites that create favorable conditions for the proliferation of various species. Figure 9(a) provides a visual representation of the relationship between the fraction of empty sites, denoted as ρ_E , and the parameter γ across various values of M . Under conditions conducive to the preservation of species diversity, specifically at $M = 10^{-5}$ and $M = 10^{-4}$, it becomes evident that the fraction of empty sites escalates in response to the incremental rise in γ , as indicated by

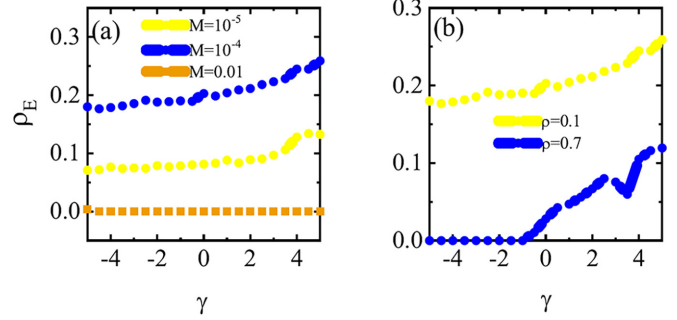


FIG. 9. The relationship between the fraction of empty sites ρ_E and the parameter γ is examined for various values of M when $\rho = 0.1$ in (a) and for different ρ values when $M = 10^{-5}$ in (b). (a) distinguishes between different M values using colors blue, yellow, and orange, representing M values of 10^{-5} , 10^{-4} , and 0.1 , respectively. Meanwhile, (b) differentiates between various ρ values using yellow and blue to denote ρ values of 0.1 and 0.7 , respectively. In the majority of cases, an increase in the fraction of empty sites is observed as γ rises.

the blue and yellow curves. In the event of species extinction, the system typically retains only two extant species, which may include one from the categories of species A , B , C , and a neutral species D . Consequently, there exists a complete occupation of network sites, rendering the fraction of empty sites equal to zero. Figure 9(b) suggests that the fraction of empty sites is higher when $\rho = 0.1$ compared to when $\rho = 0.7$.

Compared to Fig. 2, Fig. 16 in Appendix B seems that the patch's size may have an inverse relationship with γ . To explain it in detail, we provided a quantitative analysis by exploiting the basin entropy. In general, basin entropy can help us measure the unpredictability of the final state in both numerical and experimental settings for nonlinear dynamics [39,40]. The values of basin entropy range from 0 to $\log_{10}(N_A)$, where N_A represents the set of possibilities within the lattice. A zero basin entropy indicates that the system has a single attractor. On the other hand, a basin entropy of $\log_{10}(N_A)$ implies completely randomized basins with N_A equiprobable attractors. Based on the recent concept of basin entropy, we characterized the order state of the final snapshots. To be concrete, we partitioned the lattice into a set of nonoverlapping square boxes, each having dimensions $N_b \times N_b$, totaling L_b such boxes. Then the Gibbs entropy of each box S_i inside the lattice is calculated by using the equation

$$S_i = - \sum_{j=1}^{N_A} p_{ij} \log_{10} p_{ij}, \quad (4)$$

In this model, we set $N_A = 5$ since we have four species and empty sites. The value p_{ij} indicates the proportion of sites occupied by the specific species j inside the i th box. When the species inside the box are the same, we assume $p_{ij} = 0$. The basin entropy is thus obtained by

$$S_b = \frac{1}{L_b} \sum_{i=1}^{L_b} S_i, \quad (5)$$

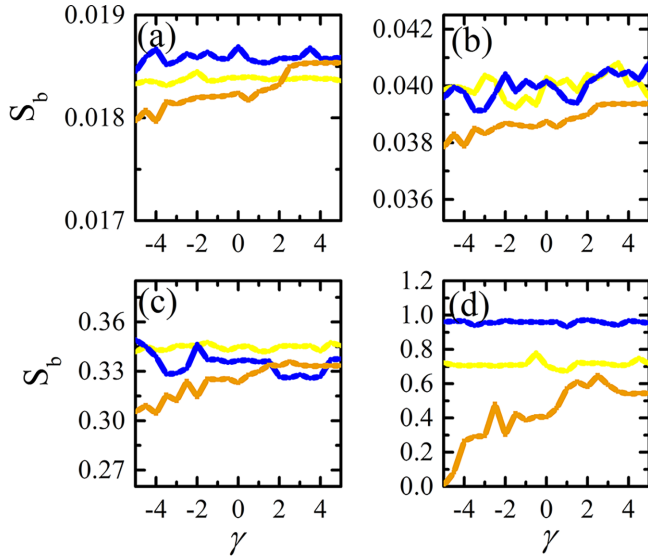


FIG. 10. Basin entropy S_b as a function of γ with different levels of N_b : (a) 4, (b) 5, (c) 10, and (d) 20. In each panel, blue and yellow curves indicate the basin entropy of $\rho = 0.1$ with different mobility values $M = 10^{-5}$ and 10^{-4} , respectively. To compare the result with different ρ , S_b of $\rho = 0.7$ (an orange curve) with $M = 10^{-5}$ is depicted at the same time. When the abundance of neutral species D is small, the difference of mobility leads to the difference in S_b , but the basin entropy shows a steady state regardless of the change of γ . As shown in orange curves, the basin entropy of $M = 10^{-5}$ with $\rho = 0.7$ increases as γ increases

As shown in Figs. 2 and 5, the spatial patterns exhibit a significant change in formation as γ is varied. To identify the significant feature, we measured the basin entropy for two cases ($\rho = 0.1$ and 0.7) presented in Fig. 10.

In Fig. 10, we depicted the relationship between S_b and γ , considering various levels of N_b . As numerically calculated, the basin entropy with γ exhibits an obvious characteristic depending on the density of D . For the low density of D , e.g., $\rho = 0.1$, variations in γ do not have an impact on the basin entropy. As shown in Fig. 10, the basin entropy with a low density of D shows a steady motion regardless of γ . However, when the abundance of D is large enough, the basin entropy increases monotonically as γ rises, as illustrated in Fig. 10. As N_b increases, the basin entropy also increases correspondingly, which aligns with previous research findings [40,41].

In summary, the spatial system exhibits different behaviors in numerical simulations for different densities of D and γ . When the density of D is small, pattern formations are consistent with traditional patterns. The role of a high γ is to create more empty sites that provide space for reproduction. Even if the density of D is high, the pattern formations get chaotic as the γ increases because the competition is stronger. The basin entropy elucidates all these phenomena. For a small fraction of D , the basin entropy remains constant even if γ changes, whereas, for a large fraction of D , the basin entropy increases as γ increases. When the number of neutral species is small, the distribution of all statuses within a small-scale box tends to be more stable. The observed state exhibits the invariance concerning stability in the parameter γ . However, when a

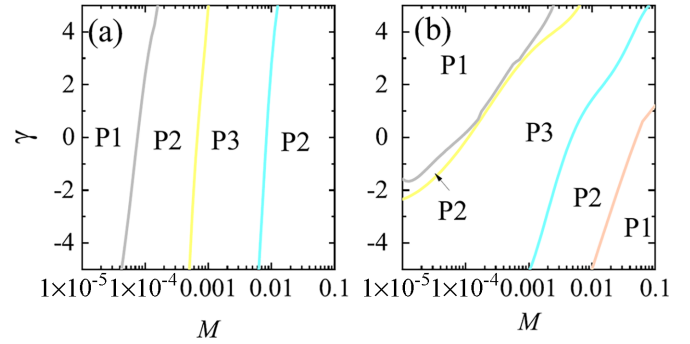


FIG. 11. Phase graph as function of M and γ . (a) and (b) present phase graphs with $\rho = 0.1$ and $\rho = 0.7$, respectively. $P1$, $P2$, and $P3$ correspond to instances of comprehensive species coexistence, partial species coexistence, and species extinction, respectively. When $\rho = 0.1$, the phase experiences four phases, when 0.7 , it experiences five phases.

significant proportion of species are neutral, the arrangement of species within boxes of the same scale becomes more disordered than that with a low proportion of D . Specifically, as the parameter γ increases, the patches or clusters of species become more fragmented, leading to a faster discretization process. Consequently, the value of entropy increases.

B. Robustness of biodiversity with neutral species

The spatiotemporal simulations presented above show that, for moderate mobility values, the system exhibits species coexistence regardless of the portion of D and the sign of γ . In addition, the snapshots also reveal the underlying mechanisms for (i) cyclic competition and (ii) forming patches by aggregating single species. While snapshots may depict the species' coexistence, the manner in which species biodiversity undergoes alterations under conditions of elevated mobility beyond the threshold at which species extinction occurs first remains enigmatic. To explore the biodiversity and the robustness as neutral species play a positive or negative role, we investigated the extinction probability incorporating M and γ with different portions of D . Since species D does not compete with other species of the RPS game, there are at least two species in the system when the species under RPS falls into the extinction state, which can also be predicted by linear stability analysis in the mean-field manner (see Appendix A for details). In simulations, when one species goes extinct, the extinction number is set to 1. To verify the robustness of the extinction probability, we obtained the results from 800 independent realizations where the extinction probability P_{ext} is defined by the proportion of the total extinction number in the total realizations.

According to phase characterization, the parameter space (M , γ) can be partitioned into distinct phases, where regions designated as $P1$, $P2$, and $P3$ correspond to instances of comprehensive species coexistence, partial species coexistence, and species extinction, respectively, see Fig. 11. Figures 11(a) and 11(b) illustrate distinct phases for ρ values of 0.1 and 0.7 , respectively. There are four turning points. To distinguish these critical thresholds, we have designated them as follows: M_{c1} , M_{c2} , M_{c3} , and M_{c4} , representing the transition

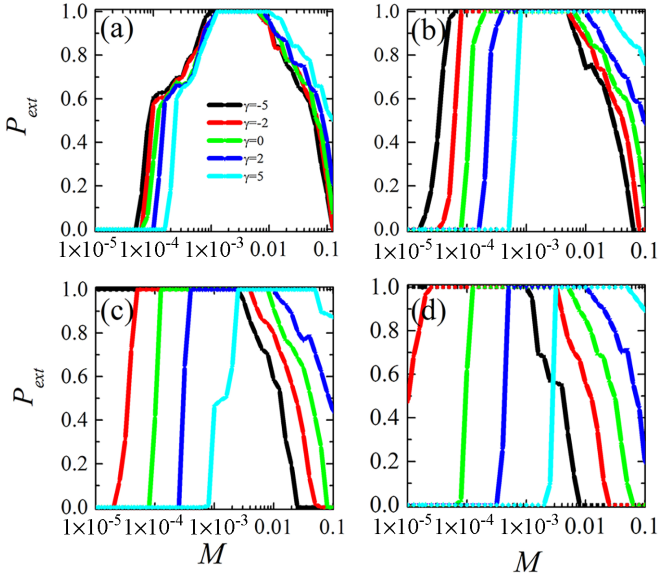


FIG. 12. Extinction probability P_{ext} as a function of mobility M with different γ where [(a)–(d)] consider the different ρ : (a) 0.1, (b) 0.25, (c) 0.5, and (d) 0.7, respectively. In each panel, different colors, black, red, green, blue, and cyan, indicate different γ : -5 , -2 , 0 , 2 , and 5 , respectively. Regardless of ρ , all panels exhibit a common feature: The increase of γ promotes coexistence accompanying the shifting threshold for breaking coexistence.

points from region $P1$ to $P2$, $P2$ to $P3$, $P3$ to $P2$, and $P2$ to $P1$, respectively. Within the region characterized by comprehensive species coexistence, a consistent presence of four species is observed. Conversely, within the area signifying species extinction, only two species persist, namely, species D , and one other species survived from the group. In the intermediate domain of partial species coexistence, the number of coexisting species can vary, with scenarios allowing for the presence of either two species (indicative of species extinction) or four species (representing complete species coexistence).

For small values of ρ and within the range of M spanning from 10^{-5} to 0.01 , the phase transitions through four distinct stages: Comprehensive species coexistence, partial species coexistence, species extinction, and, once again, partial species coexistence. In prior investigations, the entire span of M exhibited only three stages. However, here the reintroduction of partial species coexistence is facilitated by the inclusion of higher-order interactions motivated by neutral species. Simultaneously, the incorporation of higher-order interactions driven by neutral species results in a postponement of the three thresholds, namely, M_{c1} , M_{c2} , and M_{c3} , as γ increases.

For large values of ρ and within the interval of M spanning from 10^{-5} to 0.01 , the phase undergoes five discernible stages: Comprehensive species coexistence, partial species coexistence, species extinction, partial species coexistence, and comprehensive species coexistence, sequentially. Moreover, as the values of M increase, the region where area of phase $P2$ initially appears diminishes.

Figure 12 clearly shows that a larger γ advances M_{c1} at the turning point where complete coexistence is hampered,

and extinction appears. In addition, a minor γ delays M_{c1} at the turning point where the extinction state disappears, and complete coexistence appears. These phenomena are even more pronounced for a high ρ . Contrary to the previous work addressing that high mobility jeopardizes species coexistence [35], our results showed that coexistence can still be maintained at a high M . Specifically, the existence of neutral species raises the M value point, at which there is complete coexistence until extinction occurs.

Compared to the previous work of a spatial system of cyclic competition [42], we investigated the robustness of biodiversity in a broader range of mobility. We found that the extinction probability is decreasing at extremely high mobility values regardless of γ : The instability in biodiversity which is similar to Ref. [17]. Such behaviors can be comprehensive since our simulations are carried out with the normalized probability of reactions. At the high mobility regime, the normalized probability for exchange motion approaches 1 as M increases, i.e., other reactions are rare. Therefore, three species in the RPS game can have a better chance of surviving and, eventually, coexisting. Moreover, as the ρ value rises, more neutral species occupy the system, making their positive or negative effects on the cyclic competition between the three species more apparent. This leads to more significant differences in the instability characteristic of biodiversity for various γ values (see Fig. 12).

IV. DISCUSSION

In this paper, through three-way interaction, we exploited a representative non-hierarchical cyclic competition system—into which a neutral fourth species was introduced—as a tool to understand the role of neutral species. Even while the proposed model considers the evolution of four species, this is defined differently from previous studies of four species: In the previous models, all species could compete with one another [29]. In contrast, the fourth species in the proposed model, referred to as a neutral species, does not participate in the competing process. Its function merely affects the competition among the three species in the RPS system.

Since competitive reactions in the proposed model are influenced by new neutral species, we outlined several properties using spatial simulations based on knowledge of the relationship between biodiversity and reactions. In response to the simulation results, we first found that high mobility does not endanger species coexistence, contrary to the conclusions of earlier studies [10,35,43]. In addition, by observing the snapshots, we also identified two potential mechanisms that support species coexistence. The first is creating the competition cycle often seen in RPS systems. The alternative is to form patches of the same species, similar to collaborators who come together to resist aggression from defectors in evolutionary games. We further provided the basin entropy for different proportions of D to study the snapshot in-depth, and the analysis leads to the following conclusions: The basin entropy is (i) consistently maintained given the lower portion of D and (ii) increases as γ rises under the high density of D . The presence of diverse neutral species can influence the emergence of distinct system states, as

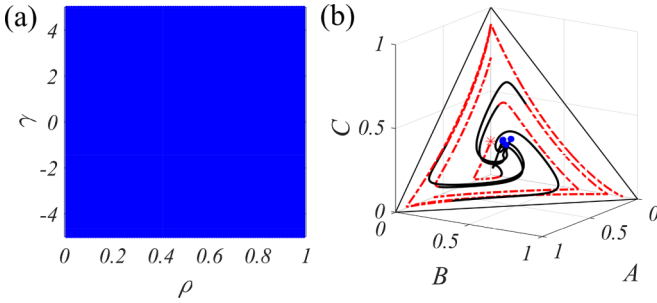


FIG. 13. Stability diagram of fixed points (A2)–(A4). Regardless of the density of D satisfying $0 < \rho < 1$, these fixed points have two negative eigenvalues that are the same as the classic RPS system [35], as in (a), and Eq. (A1) ultimately exhibits asymptotically stable heteroclinic cycles as shown in (b). In particular, the blue area in (a) indicates that eigenvalues $\lambda_{2,3}$ are always negative regardless of ρ and γ .

manifested by the observed basin entropy. Hence, for $\rho = 0.1$, the basin entropy remains constant as the parameter γ varies. However, in scenarios with a high density of neutral species, the basin entropy shows an increasing trend as the γ increases.

This paper has some limitations. The first one is that more complex competing processes are not taken into account [44,45]. The consideration of neutral species in these models may further complicate the relationship. Second, we ignored the effects of mutations. Even with such limitations, we could confirm the effect of neutral species on biodiversity through the RPS model governed by higher-order interaction. As a result, we believe that our results could provide a fundamental basis for elucidating the influence of neutral and top herbivores in ecosystems.

ACKNOWLEDGMENTS

We acknowledge the support provided by the Major Program of National Fund of Philosophy and Social Science of China (Grants No. 22&ZD158 and No. 22VRCO49) to L.S. Y.L. was supported by the National Natural Science Foundation of China Project No. 32160239. J.P. was supported by the National Research Foundation of Korea (NRF) grant funded by the Korea government (MSIT) (No. NRF-2021R1A4A1032924 and No. NRF-2023R1A2C1004893). We acknowledge support from Yunnan Provincial Department of Education Science Research Fund Project (Grant No. 2023Y0620). Y.N.G. was funded by the Science Research Project of Education Department of Hunan Province (Grant No. 22C0014). Y.L. and Y.W. were funded by the China Scholarship Council for a one-year study at the University of Zaragoza.

APPENDIX A: MACROSCOPIC APPROACH THROUGH ODES

In our model, since neutral species D always exists and has an effect on interspecific competition, investigating fixed points can be possible by focusing on the behavior of three species A , B , and C . On a mean-field level, the local density of species D , ρ_i/k , can be regarded as ρ , and the deterministic

system incorporating reactions (1) and (2) with $q = 1$ can be written,

$$\begin{aligned} \frac{da}{dt} &= a(t)[(1 - \rho_0) - e^{\gamma\rho}c(t)], \\ \frac{db}{dt} &= b(t)[(1 - \rho_0) - e^{\gamma\rho}a(t)], \\ \frac{dc}{dt} &= c(t)[(1 - \rho_0) - e^{\gamma\rho}b(t)], \end{aligned} \quad (\text{A1})$$

for the well-mixed population ($N \rightarrow \infty$). In the above equations, $1 - \rho_0$ is the fraction of empty sites.

Equation (A1) possesses four different fixed points: (i) three absorbing points for the survival of two species and (ii) the internal point for the coexistence of all species, which are listed as follows:

(1) Survival of two species:

$$(a^*, 0, 0, d^*) = (1 - \rho, 0, 0, \rho), \quad (\text{A2})$$

$$(0, b^*, 0, d^*) = (0, 1 - \rho, 0, \rho), \quad (\text{A3})$$

$$(0, 0, c^*, d^*) = (0, 0, 1 - \rho, \rho). \quad (\text{A4})$$

(2) Coexistence of all species:

$$(a^*, b^*, c^*, d^*) = \left(\frac{1 - \rho}{A'}, \frac{1 - \rho}{A'}, \frac{1 - \rho}{A'}, \rho \right), \quad (\text{A5})$$

where $A' = 3 + e^{\gamma\rho}$.

On a macroscopic level, the stability of each fixed point can be investigated by Jacobian arguments, where the Jacobian matrix \mathbf{J} of Eq. (A1) at point \mathbf{x} is defined,

$$\mathbf{J}(\mathbf{x}) = \begin{bmatrix} J_{11} & -a & -a - e^{\gamma\rho}a \\ -b - e^{\gamma\rho}b & J_{22} & -b \\ -c & -c - e^{\gamma\rho}c & J_{33} \end{bmatrix}, \quad (\text{A6})$$

where the components J_{ii} ($i \in \{1, 2, 3\}$) are given by

$$J_{11} = 1 - 2a - b - c - \rho - e^{\gamma\rho}c,$$

$$J_{22} = 1 - a - 2b - c - \rho - e^{\gamma\rho}a,$$

$$J_{33} = 1 - a - b - 2c - \rho - e^{\gamma\rho}b.$$

For fixed points (A2)–(A4), they have eigenvalues:

$$\lambda_1 = 0, \quad \lambda_2 = \rho - 1, \quad \lambda_3 = e^{\gamma\rho}(\rho - 1).$$

Since $0 < \rho < 1$, it is obvious that eigenvalues $\lambda_{2,3}$ are negative, and hence these fixed points may constitute heteroclinic cycles that are asymptotically stable. The characteristic of these absorbing fixed points is similar to that in classic RPS systems, and thus Eq. (A1) shows asymptotically stable heteroclinic cycles as shown in Fig. 13(b).

For the fixed point (A5), the corresponding eigenvalues are

$$\lambda_1 = \rho - 1, \quad \lambda_{2,3} = \frac{(1 - \rho)e^{\gamma\rho}}{2(3 + e^{\gamma\rho})}(1 \pm \sqrt{3}i).$$

Since $0 < \rho < 1$, it is trivial that $\lambda_1 < 0$. For $\lambda_{2,3}$, the two eigenvalues have positive real parts, i.e., $\text{Re}(\lambda_{2,3}) > 0$. Thus, the fixed point (A5) is always unstable.

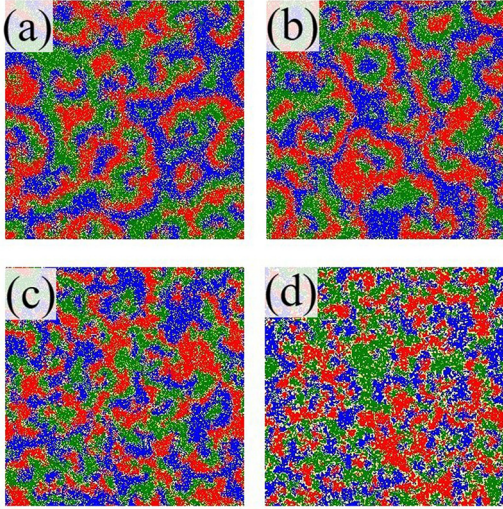


FIG. 14. Typical snapshots for fixed parameters $M = 10^{-5}$ and $\rho = 0.1$ with different γ : (a) -5 , (b) -2 , (c) 2 , and (d) 5 , which are obtained from the 712 200th time step. Four species A, B, C, D , and empty sites are indicated by red, blue, green, yellow, and white, respectively. As γ increases, there seem to be no significant differences in the spiral patterns.

APPENDIX B: THE RESULT OF M BEING 10^{-5}

Here we present the snapshots obtained with $M = 10^{-5}$ for various values of γ , as shown in Fig. 14.

In this particular condition, Figs. 14(a)–14(d) demonstrate that varying γ does not significantly affect the spatial pattern. In all cases, we discern a rise in the quantity of vacant sites attributable to the heightened competition strength at low levels of mobility.

Additionally, in Fig. 15, we present the time-dependent evolution of species and empty sites. The results demonstrate

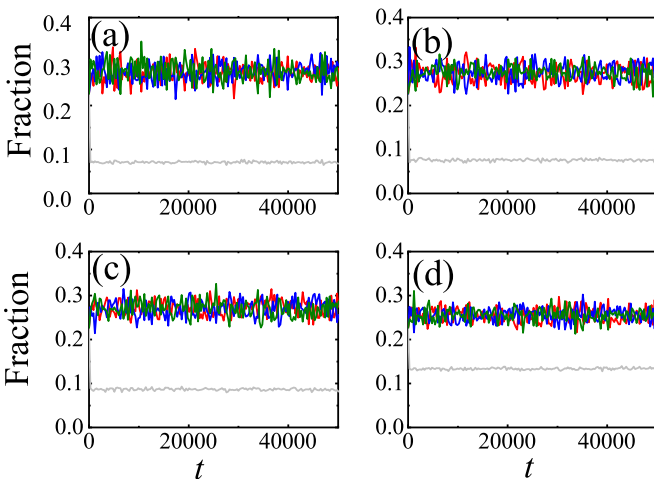


FIG. 15. Time-dependent evolution of densities for $M = 10^{-5}$ and $\rho = 0.1$ with different γ : (a) -5 , (b) -2 , (c) 2 , and (d) 5 . Red, blue, green, and grey lines represent species A, B, C , and empty sites. The increase in γ intensifies interspecific competition and consequently increases the fraction of empty sites.

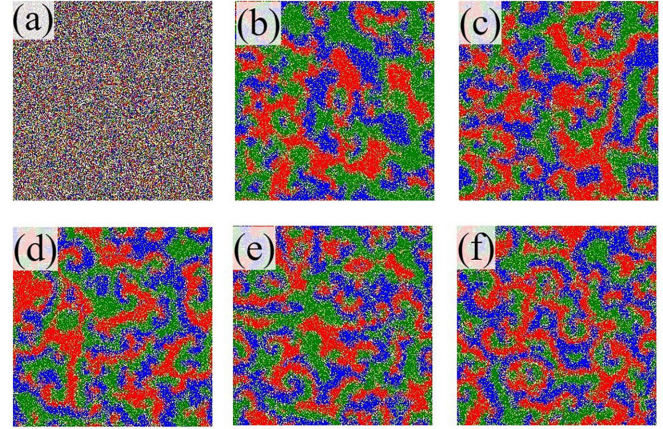


FIG. 16. Evolutionary snapshots for fixed parameters $M = 10^{-5}$, $\gamma = -2$, and $\rho = 0.1$ with different time steps: (a) 1, (b) 1 200 000, (c) 1 393 000, (d) 1 430 000, (e) 1 699 000, and (f) 1 900 000. Under conditions of low mobility, the formation of discontinuous spiral waves becomes feasible.

that the fraction of species exhibits dynamic stability through a cyclic competitive process.

Figure 16 presents a series of evolutionary snapshots. To be concrete, Fig. 16(a) shows the initial distribution of all species and empty sites. As time progresses, as shown in Fig. 16(b), the species gather together and form an inconspicuous spiral pattern of competition within a short period [see Figs. 16(c)–16(f)].

After analyzing the microscopic and evolutionary traits of species under the conditions $\rho = 0.7$ and $M = 10^{-4}$ in Figs. 5–7, we present the corresponding outcomes for $M = 10^{-5}$ which are depicted in Figs. 17 and 18. However, for $\gamma > 0$, a more robust competition rate leads to a dispersion of species. Specifically, higher values of γ promote

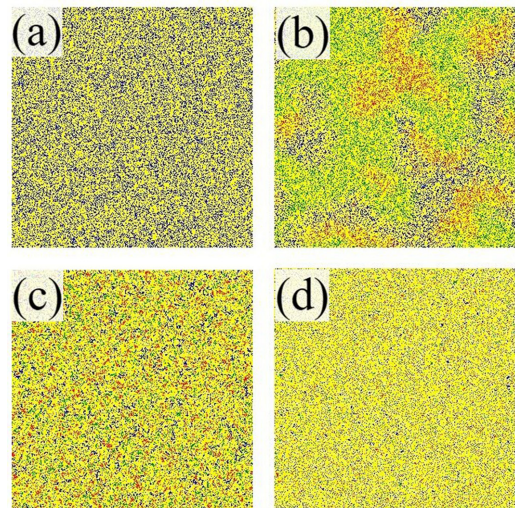


FIG. 17. Typical snapshots for fixed parameters $M = 10^{-5}$ and $\rho = 0.7$ with the 712 200th time step. The panel construction for parameter γ is the same as Fig. 14. Since the density of D is moderately high, all panels seem occupied by it. In this case, the spatial patterns transfer from order to disorder as γ increases.

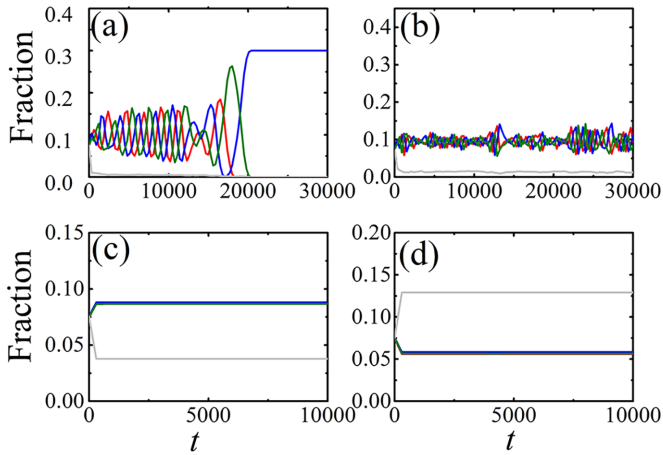


FIG. 18. Time-dependent evolution of densities for $M = 10^{-5}$ and $\rho = 0.7$ with different γ : (a) -5 , (b) -2 , (c) 2 , and (d) 5 . The color indications are the same as Fig. 15. The increase in γ intensifies interspecific competition and consequently increases the fraction of empty sites.

the presence of discrete species. The presence of neutral species further contributes to the separation of different species. A higher γ accelerates the competition process, reducing cluster sizes and increasing the fraction of empty sites.

These patterns in Fig. 17 correspond to distinct temporal evolutionary patterns of species (see Fig. 18). In one scenario, species go extinct; in another, different species engage in cyclic competition. The third scenario involves the separation of different species by neutral species, leading to the

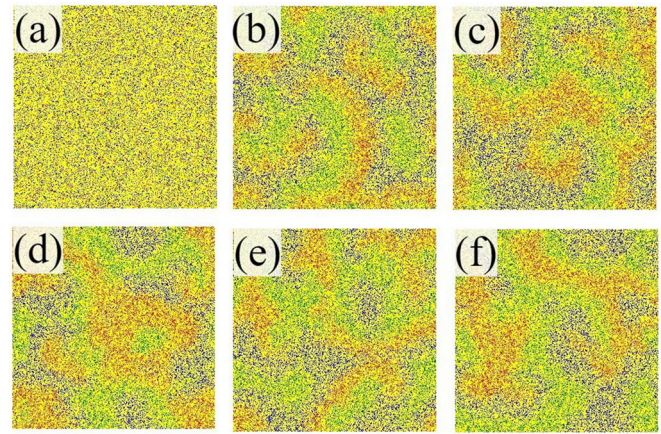


FIG. 19. Typical snapshots for fixed parameters $M = 10^{-5}$ and $\rho = 0.7$ at different time steps: (a) 1, (b) 23 000, (c) 193 000, (d) 2 260 000, (e) 2 330 000, and (f) 2 400 000. Species participating in the RPS game are embedded in D to form patches.

stabilization of the species fraction over a short period. A higher value of γ decreases the species fraction and promotes the production of empty sites.

Figure 19(a) exhibits that species A , B , C , and empty sites are embedded arbitrarily in D for $\rho = 0.7$ at the initial stage. And as shown in Figs. 19(b) and 19(c), we further discovered that spiral waves appear under the rules of the species competition cycle. As time goes by, however, the spiral waves disappear, and species form patches embedded in D [see Figs. 19(d)–19(f)].

-
- [1] M. M. Mayfield and D. B. Stouffer, *Nat. Ecol. Evol.* **1**, 0062 (2017).
- [2] S. Basu, K. Kumbier, J. B. Brown, and B. Yu, *Proc. Natl. Acad. Sci. USA* **115**, 1943 (2018).
- [3] P. Singh and G. Baruah, *Theor. Ecol.* **14**, 71 (2021).
- [4] J. M. Levine, J. Bascompte, P. B. Adler, and S. Allesina, *Nature (London)* **546**, 56 (2017).
- [5] J. Grilli, G. Barabás, M. J. Michalska-Smith, and S. Allesina, *Nature (London)* **548**, 210 (2017).
- [6] A. Swain, L. Fussell, and W. F. Fagan, *Proc. Natl. Acad. Sci. USA* **119**, e2020956119 (2022).
- [7] H. Guo, D. Jia, I. Sendiña-Nadal, M. Zhang, Z. Wang, X. Li, K. Alfaro-Bittner, Y. Moreno, and S. Boccaletti, *Chaos, Solitons Fractals* **150**, 111103 (2021).
- [8] E. Bairey, E. D. Kelsic, and R. Kishony, *Nat. Commun.* **7**, 12285 (2016).
- [9] J. Park, *Chaos* **29**, 071107 (2019).
- [10] J. Park and B. Jang, *Appl. Math. Comput.* **394**, 125794 (2021).
- [11] Y. Lu, C. Shen, M. Wu, C. Du, L. Shi, and J. Park, *Chaos* **32**, 081104 (2022).
- [12] Y. Lu, X. Wang, M. Wu, L. Shi, and J. Park, *Chaos* **32**, 093116 (2022).
- [13] M. H. Mohd and J. Park, *Chaos, Solitons Fractals* **153**, 111579 (2021).
- [14] B. Sinervo and C. M. Livel, *Nature (London)* **380**, 240 (1996).
- [15] J. B. C. Jackson and L. Buss, *Proc. Natl. Acad. Sci. USA* **72**, 5160 (1975).
- [16] C. E. Paquin and J. Adams, *Nature (London)* **306**, 368 (1983).
- [17] T. Reichenbach and E. Frey, *Phys. Rev. Lett.* **101**, 058102 (2008).
- [18] J. Park, Y. Do, B. Jang, and Y.-C. Lai, *Sci. Rep.* **7**, 7465 (2017).
- [19] X. Ni, R. Yang, W.-X. Wang, Y.-C. Lai, and C. Grebogi, *Chaos* **20**, 045116 (2010).
- [20] X. Wang, Y. Lu, L. Shi, and J. Park, *Sci. Rep.* **12**, 1821 (2022).
- [21] J. Park, *Chaos* **29**, 033102 (2019).
- [22] M. J. Liao, A. Miano, C. B. Nguyen, L. Chao, and J. Hastly, *Nat. Commun.* **11**, 6055 (2020).
- [23] B. Moura and J. Menezes, *Sci. Rep.* **11**, 6413 (2021).
- [24] R. Baker and M. Pleimling, *J. Theor. Biol.* **486**, 110084 (2020).
- [25] J. Park, Y. Do, Z.-G. Huang, and Y.-C. Lai, *Chaos* **23**, 023128 (2013).
- [26] S. Bhattacharyya, P. Sinha, R. De, and C. Hens, *Phys. Rev. E* **102**, 012220 (2020).
- [27] D. Bazeia, B. F. de Oliveira, J. V. O. Silva, and A. Szolnoki, *Chaos, Solitons Fractals* **141**, 110356 (2020).
- [28] P. P. Avelino, B. F. de Oliveira, and R. S. Trintin, *Phys. Rev. E* **100**, 042209 (2019).
- [29] M. Frean and E. R. Abraham, *Proc. R. Soc. Lond. B* **268**, 1323 (2001).

- [30] S. Chatterjee, S. Nag Chowdhury, D. Ghosh, and C. Hens, *Chaos* **32**, 103122 (2022).
- [31] M. Rees and K. E. Rose, *Proc. R. Soc. Lond. B* **269**, 1509 (2002).
- [32] H. F. Lamprey, *African J. Ecol.* **1**, 63 (1963).
- [33] D. Bazeia, M. Bongestab, B. F. de Oliveira, and A. Szolnoki, *Chaos, Solitons Fractals* **151**, 111255 (2021).
- [34] D. Bazeia, B. F. de Oliveira, and A. Szolnoki, *Europhys. Lett.* **124**, 68001 (2018).
- [35] T. Reichenbach, M. Mobilia, and E. Frey, *Nature (London)* **448**, 1046 (2007).
- [36] S. Redner, *A Guide to First-Passage Processes* (Cambridge University Press, Cambridge, UK, 2001).
- [37] Z. Zhu, Y. Dong, Y. Lu, and L. Shi, *Physica A* **569**, 125772 (2021).
- [38] C. Du, K. Guo, Y. Lu, and L. Shi, *Appl. Math. Comput.* **438**, 127617 (2023).
- [39] A. Daza, A. Wagemakers, B. Georgeot, D. Guéry-Odelin, and M. A. Sanjuán, *Sci. Rep.* **6**, 31416 (2016).
- [40] M. Mugnaine, F. Andrade, J. Szezech, and D. Bazeia, *Europhys. Lett.* **125**, 58003 (2019).
- [41] B. Jiang, L. Yuan, R. Zou, R. Su, and Y. Mi, *Chaos, Solitons Fractals* **170**, 113411 (2023).
- [42] S. Islam, A. Mondal, M. Mobilia, S. Bhattacharyya, and C. Hens, *Phys. Rev. E* **105**, 014215 (2022).
- [43] L.-L. Jiang, W.-X. Wang, Y.-C. Lai, and X. Ni, *Phys. Lett. A* **376**, 2292 (2012).
- [44] A. Roman, D. Dasgupta, and M. Pleimling, *J. Theor. Biol.* **403**, 10 (2016).
- [45] S. Esmacili, B. L. Brown, and M. Pleimling, *Phys. Rev. E* **98**, 062105 (2018).